# Ultra-compact microstructured methane steam reformer with integrated Palladium membrane for on-site production of pure hydrogen: Experimental demonstration

*T. Boeltken, A. Wunsch, T. Gietzelt, P. Pfeifer*[*], *R. Dittmeyer*

*Institute for Micro Process Engineering (IMVT), Karlsruhe Institute of Technology (KIT), Hermann von Helmholtz Platz 1, 76344 Eggenstein Leopoldshafen, Germany*

*Keywords:*
Microstructured membrane reactor
Palladium membrane
Methane steam reforming
Rh based catalyst
Compact system
Laser welding

A B S T R A C T

A novel metal based modular microstructured reactor with integrated Pd membrane for hydrogen production by methane steam reforming is presented. Thin Pd foils with a thickness of 12.5 μm were leak tight integrated with laser welding between micro structured plates. The laser welded membrane modules showed ideal $H_2/N_2$ permse lectivities between 16,000 and 1000 at 773 K and 6 bar retentate pressure. An additional metal microsieve support coated with an YSZ diffusion barrier layer (DBL) facilitated the operation at temperatures up to 873 K and pressures up to 20 bar pressure difference. The membrane permeability in this configuration is expressed with Q = 1.58E 07*exp( 1460.2/T) mol/(msPa$^{0.5}$).

In the first proof of concept reaction experiments the influence of W/F ratio (0.33 1.32 $g_{Cat}h/mol_{CH_4}$), S/C ratio (3 and 4), temperature (773 and 823 K) and retentate/reformate pressure (6 12 bar) was studied. Methane conversion of 87% and a hydrogen recovery of 92% were obtained at a W/F ratio of 0.33 $g_{Cat}h/mol_{CH_4}$, corresponding to a GHSV of 29,000 h $^{1}$, a temperature of 823 K and a feed pressure of 12 bar without the use of sweep gas.

The microstructured membrane reactor showed a promising performance for the production of pure hydrogen in a very compact and modular system.

## Introduction

The process intensification potential of compact reactors with integrated Pd based membranes for distributed production of pure hydrogen by steam reforming of natural gas or methane (MSR) has been highlighted in recent publications [1,2]. The approaches to apply innovative reactor types refers to tech nical solutions, where on site hydrogen production is favored instead of delivery of hydrogen in compressed or liquefied state via truck transportation.

The Pd based membrane selectively separates the hydrogen from the reactor in high purity. In consequence, further complex purification steps, such as pressure swing

* *Corresponding author*. Tel.: +49 (0) 721 60824767.
E mail address: peter.pfeifer@kit.edu (P. Pfeifer).

adsorption (PSA) are elided. Additionally, the membrane is improving reaction kinetics of the steam reforming (Eq. (1)), and the concurrent water gas shift (Eq. (2)) by shifting the thermodynamic equilibrium due to the extraction of hydrogen from the reaction zone. As a consequence, reaction temperatures can be decreased, while maintaining high conversion [3].

$$CH_4 + H_2O \leftrightarrow CO + 3H_2 \quad \Delta H^0_{298K} \quad 206\ kJ/mol \tag{1}$$

$$CO + H_2O \leftrightarrow CO_2 + H_2 \quad \Delta H^0_{298K} \quad 41\ kJ/mol \tag{2}$$

In literature, tubular membranes with diameters of around 2–10 mm with catalyst particles supplied as a packed bed around the membrane tube are frequently described [2–6].

However, for an optimized system efficiency, and high catalyst and membrane utilization several design parameters of a membrane reactor need to be considered:

- A sufficiently large membrane area per catalyst volume is required to achieve a good match of hydrogen production rate and hydrogen flux through the membrane [7], given the case that the activity of the catalyst is high enough to keep up with the shift of the thermodynamic equilibrium.
- The gas transport of generated hydrogen from and through the hydrogen producing catalyst bed may be significantly limited (concentration polarization) [8]. This results in a reduced driving force for hydrogen permeation, and a lower utilization of the Pd membrane when the hydrogen flux through the membrane is high. The application of thin membranes for reducing the system costs is consequently increasing the importance of this aspect.
- Good heat integration is crucial for the endothermic steam reforming reaction. Heat transfer limitation results in more fuel consumption for the burners and temperature gradi ents can have a remarkable effect on the overall system performance.

Tubular membrane reactors with large diameters offer a relatively small membrane area to catalyst volume ratio. Even when a membrane tube of only 1 cm in diameter is considered with an internal catalyst bed, only 400 $m^2/m^3$ of membrane surface area can be supplied. For high reaction rates and/or high permeance, this might not be sufficient.

In general, the mass transfer resistance in the gas phase is significantly reduced the closer membrane surface and cata lyst are brought in contact [9]. However, direct contact be tween catalyst and membrane surface has to be avoided to prevent mechanical damage of the membrane or undesired reactions by active site membrane contact.

More elaborate designs are described in literature to counteract the effect of concentration polarization. Van Sint Annaland and co workers presented a (micro) fluidized bed membrane reformer for the autothermal reforming of methane with reduced mass transfer resistance between catalyst and membrane, and potential hot spots are avoided as well [10,11].

A research group of KIERS in Korea reported a planar cir cular membrane module integrated in a housing and $H_2$ re covery could be increased by decreasing the distance between module wall and membrane surface from 2.5 mm to 0.4 mm [12,13]. Based on this design, a modular disk type multi membrane reformer for hydrogen production from methane steam reforming was presented that operates at pressures up to 21 bar [14].

Tokyo Gas has developed the world's largest membrane reformer so far for the production of 40 $Nm^3H_2/h$ from natural gas, and an efficiency of 81.4% was reported [15]. In this sys tem, structured catalyst modules are used that are attached close to the membrane surface [16].

Microstructured reactors are characterized by high indi rect heat exchange and high mass transfer rates, and are well documented in the literature [17,18]. The small lateral di mensions of the microchannels result in a large surface area to volume ratio, a feature that makes the incorporation of thin membranes attractive [19]. For example, microchannels with a channel depths of 200 μm coated with a catalyst layer of 10 μm inside the channel would result in a membrane surface area to catalyst volume ratio of 100,000 $m^2/m^3$, pro vided that every microstructured catalyst foil is in contact with the membrane. Due to this very high ratio, extremely active catalysts can be used to produce hydrogen at a rate comparable to the hydrogen removal rate through the membrane [20]. A membrane surface area to catalyst volume ratio of 100,000 $m^2/m^3$, however, may be too high for practical applications, and therefore the design of a microstructured membrane reactor should be adapted to the process needs in order to neither oversupply Pd membrane area nor expensive catalytic material. The small dimensions of the micro channels will minimize mass transfer effects towards the membrane [9]. Furthermore, up scaling of this reactor type is possible by stacking multiple microstructured elements to a modular reactor. Hence, very compact systems are anticipated.

MEMS type membrane integrated microreactors based on silicon and glass have been proven to produce hydrogen from steam reforming and partial oxidation of methanol [21,22]. For example, methanol conversion of up to 63% was obtained at 475 °C and atmospheric pressure, and hydrogen permeation through a 200 nm thin Pd–Ag alloy film resulted in a hydrogen recovery of 47% [22]. The pressure difference for these ultra thin membranes was limited to 70 kPa and challenges, such as sealing of the metal membrane with the silicon based device and membrane stability at elevated pressures and temperatures remain. However, this chip like membrane reactor type is interesting for fueling fuel cells in the Watt and sub Watt range for portable applications [21,23].

A further step towards a technical system is an approach that originates from thin metallic plate type heat ex changers that carry microchannels in the micrometer range and are coated with a catalyst layer or filled with a micro packed bed. The advantage of metallic microreactors is that there is a variety of techniques available for bonding of metals [24]. Each bonding technique has to be well matched with the process parameters of the application of the device. Full faced connections between the thin metallic foils can be achieved with diffusion bonding in vacuum at elevated temperatures close to the Tammann temperature, where self diffusion processes of the crystals bond the metal parts. Pressing load and time influence the bonding result as well.

The major advantage of this method is the extremely high pressure resistance of the bonded device. On the other hand, this bonding method requires high mechanistic build up and time consuming batch procedure, and a heat treat ment of the entire microstructured device is the conse quence. Due to the high temperatures applied, this method is apparently not suitable for bonding of metallic foils with coated surfaces, such as previously catalyst coated micro channels, or for the integration of thin membranes. Furthermore, the pressing load and the bonding temperature are interrelated, and comprehensive test weldings are consequently required [25].

Welding processes with a localized heat affected zone, such as electron beam or laser welding are very interesting for the fabrication of microstructured devices with previously indicated requirements. If applicable, certain pressure absorbing housings have to be utilized, as in most cases only the circumference of the welding is accessible. In return, different metallic materials or metallic stacks with interme diate layers can be joined. Furthermore, similar materials, such as austenitic stainless steel and nickel based alloys can be welded with the identical parameters [26].

In contrast to electron beam welding, where the required energy is introduced into the material by highly accelerated electrons in a vacuum, the application of a laser brings further advantages. In particular, solid state lasers can combine high energy densities, narrow seam geometry with high aspect ratio (depth/width of weld seam), low energy input per unit length and therefore a low thermal strain with marginal deformation, good weld seam quality and high level of auto mation in an inert atmosphere. Depending on the heat con ductivity of the material and the welding speed, the heat influence on the material can be minimized. Requirements for the deep weld effect is the formation of a metal vapor plasma at power densities of around $10^6$ W/cm$^2$.

A highly precise laser welding technique, a planar stack of microchannel foils, together with membrane foils and addi tional supports was used in this work to produce and to vali date the concept of a modular, scalable and very compact metallic membrane microreactor.

## Experimental

### *Design of the stacked microstructured membrane reactor – the μ-EnH$_2$ancer*

The reformer consists of a housing with inlets for methane and water and the (optional) sweep gas, as well as outlets for the reformate and the separated hydrogen. The reactor housing can be equipped with one or multiple membrane modules, depending on the hydrogen production capacity. Each membrane module is leak tight integrated by laser welding and the layout of the $\mu$ EnH$_2$ancer is shown in detail in Fig. 1(a and b). The laser welded membrane modules are sealed with each other with graphite rings to enable replace ment of singular modules in case of membrane defects. High temperature resistant metal alloy (Nicrofer® 3220H/Alloy 800 (1.4876), ThyssenKrupp, Germany) was used as material for the housing and the membrane modules. The stacking prin ciple of the $\mu$ EnH$_2$ancer is shown in Fig. 1(a).

Fig. 1(b) shows a schematic view of the microstructured membrane module. Each module consists of a "pre reform ing" zone, where methane or natural gas is converted with water vapor and ideally a hydrogen partial pressure slightly greater than the permeate pressure is generated to avoid back permeation from the permeate side of the membrane. The subsequent reforming zone is in contact with the Pd based membrane which separates and purifies the generated $H_2$ and further enhances the methane conversion and the hydrogen recovery along the microchannel. In this work, the reactor is electrically heated by cartridges, but heating by combustion of the retentate is anticipated in the future.

The microchannels were prepared by wet chemical etching. The "pre reforming" zone consists of 75 micro channels with a width × depth × length of 500 μm × 300 μm × 50 mm, and the microchannels of the "reforming" zone, i.e. the one in contact with the membrane, differ only in length (70 mm). The microstructured foils have a thickness of 1 mm, but 0.5 mm in a future optimized version is anticipated.

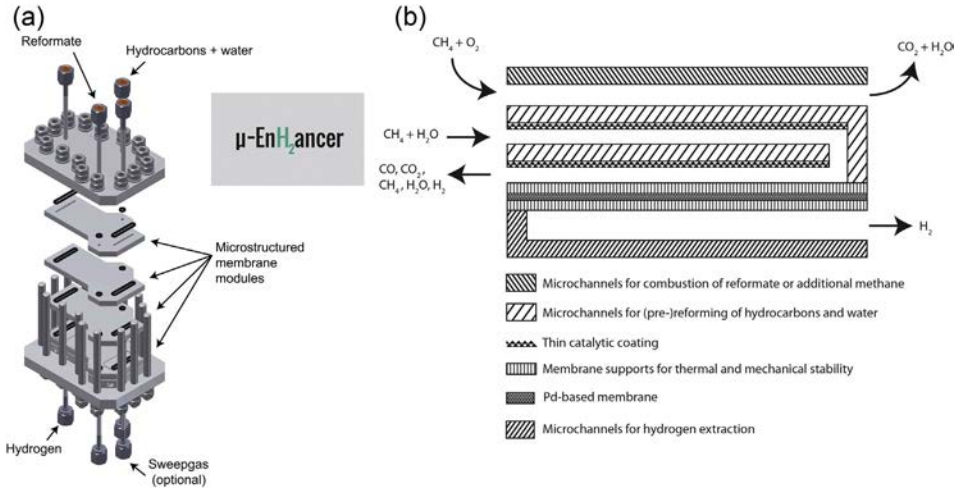


**Fig. 1 – Stacking principle of modular microstructured membrane reactor a), schematic illustration of the channel configuration in the microchannel membrane module, here shown with heat integration by combustion b).**

Etched microsieve stainless steel foils (material 1.4301), with a thickness of 50 μm, and holes with a diameter of 140 μm (80 μm gap between the holes) were used as additional stabi lizing support on both sides of the membrane to avoid mem brane rupture due to pressure fluctuations. The support side allocated to the membrane surface was coated with a thin (<1 μm) yttria stabilized zirconia layer by magnetron sput tering. Two functions are fulfilled by the supports. First, the etched holes decrease the mechanical stress on the mem brane, while the YSZ coating acts as a barrier layer against intermetallic diffusion at elevated temperatures from the metallic support into the Pd membrane. In the experiments of this work, a 12.5 μm thin Pd membrane was used. The mem brane was supplied by Hauner Metallische Werkstoffe (HMW), Germany.

### *Preparation of the catalyst coating*

The catalyst support coating slurry was prepared with aluminum oxide nanoparticles admixed with a sol–gel solu tion. The aluminum oxide nanoparticles generate the catalyst mass, while the sol–gel enhances the adhesion of the support on the microchannel foils. A sol is composed of metal alkox ides that form a metal hydroxide group through hydrolysis. Due to polycondensation processes the desired particles are formed. First, 6.2 g Aluminum sec butylat (Alfa Aesar, 97%) were dissolved in 20 ml isopropanol and simultaneously 2.5 g acetyl acetone (Merck, 99%) was dissolved in 10 ml iso propanol. Both solutions were mixed and then stirred for 30 min. To start the hydrolysis 0.9 g of $H_2O$ in 10 ml of iso propanol was added to the solution with another stirring for 30 min. Then nitric acid ($HNO_3$, BDH Prolabo, 60%) is drop wise added to the solution until pH 3.5 is reached [27]. Subse quently, alumina nanoparticles (mixture of $\alpha$ phase and $\gamma$ phase, particle diameter of 300 nm), 99.99% (metal basis), Alfa Aesar, were mixed with ethanol to a 20 wt.% dispersion. The dispersion was stirred for 30 min before the sol in the same amount of ethanol was added. Finally, the dispersion was stirred for another 24 h [28]. The dispersion was then impregnated manually with a pipette from the top on the microchannel foils (5 $\mu l/mm^3$ of channel volume), dried at 90 °C in an oven over night and then calcined at 1073 K for 6 h (heating rate 2 K/min).

An aqueous Rh solution with a concentration of 22.8 $g_{Rh}/l$ was prepared, starting from Rhodium(III) nitrate hydrate ($Rh(NO_3)_3{}^*xH_2O$; Rh % 35.14%), Chempur Feinchemikalien und Forschungsbedarf GmbH, Germany. The Rh concentra tion of the solution was determined after dilution with ICP OES. For the preparation of the catalytic coatings, the alumina support in the microchannels was manually impregnated with 0.71 $\mu l_{Rh\ solution}/(mm^3_{Channel})$, correspond ing to 15 wt.% Rh with respect to $Al_2O_3$. Finally the catalysts were calcined at 1023 K for 6 h (heating rate 2 K/min).

### *Laser welding of microstructured membrane modules*

In this work a TruLaser Cell 3010 (Trumpf, Germany) was used. The tool machine has a positioning accuracy of ±15 μm, a high dynamic of 10 $m^2/s$ of the axis and a maximum speed of 50 m/ min. It is connected to a Yb YAG disk laser TruDisk 3001 (Trumpf, Germany), with a maximum power of 3 kW, and a light conducting cable with a diameter of 100 μm. Optionally, a light conducting cable with a diameter of 400 μm has been integrated in a second outlet. A focal distance of $f$ 150 mm was used.

The stack was assembled by through penetration welding of two sheets from above. By appropriate lateral variation of the welding paths, the passages could be separated from each other. Attention has to be paid to the clamping of several layers during through penetration welding to obtain high vacuum prove welding seams: Gaps between layers must be avoided since these represent a strong thermal insulation, preventing reproducible and predictable welding seam ge ometry or promote shrinking holes and crack formation in the surface of the weld seam. The same applies for layers with an oxidized surface: parameter tests must be performed to ascertain reasonable welding depth and cross section of the weld seam. Other issues are the impact of the design of the apparatus and the welding parameters on the thermal field during welding to prevent distortion or crack formation in the thin membranes in terms of rate of heat conductivity of the apparatus. The same deposited energy per unit of length ob tained with different welding parameters leads not neces sarily to comparable welding results. Even successful parameters may not perform for different designs.

### *Test rig and gas analytics*

The simplified flow chart of the test rig is shown in Fig. 2. Mass flow controllers (MFC, Brooks Instrument, Model 5850S) were used for the dosage of gaseous components. A liquid flow controller (LFC, Brooks Instrument, Model FLΩMEGA® Model 5881) and a microstructure nozzle evaporation technique was used for continuous and pulsation free water supply [29]. The water was atomized and evaporated together with $CH_4$. The pipes of the test rig were electrically heated with heating coils.

The pressure was adjusted with two high pressure valves (Flowserve, Kammer Ventile). The microstructured mem brane reactor was installed into the test rig and seven heating cartridges and four thermocouples on each side of the housing (see Fig. 1) were used for temperature control and measure ment. The pressure drop along the microchannels was negli gible (<100 mbar) and the temperature difference along the reactor housing was always less than 5 K.

The inlet concentration of the feed was adjusted in bypass, while the reactor was flushed with $N_2$ or $H_2$ on retentate side, and with $N_2$ on the permeate side. Gas concentrations of the retentate were analyzed with a gas chromatograph (GC, Agi lent Technologies 7890A and 6890A) equipped with a metha nation unit, a thermal conductivity detector (TCD) and a flame ionization detector (FID). The gas concentration of the permeate was not analyzed at all times, as most of the ex periments were conducted without the use of sweep gas. In this case, the permeate flow was measured with a bubble flow meter. Given the case that sweep gas was used, the volume flow of $H_2$ across the membrane was calculated according to gas concentrations determined by GC analysis (Agilent Tech nologies 6890A, identical equipment as above). In this configuration, hydrogen purity was calculated based on car bon containing species in the permeate, see Eq. (8).

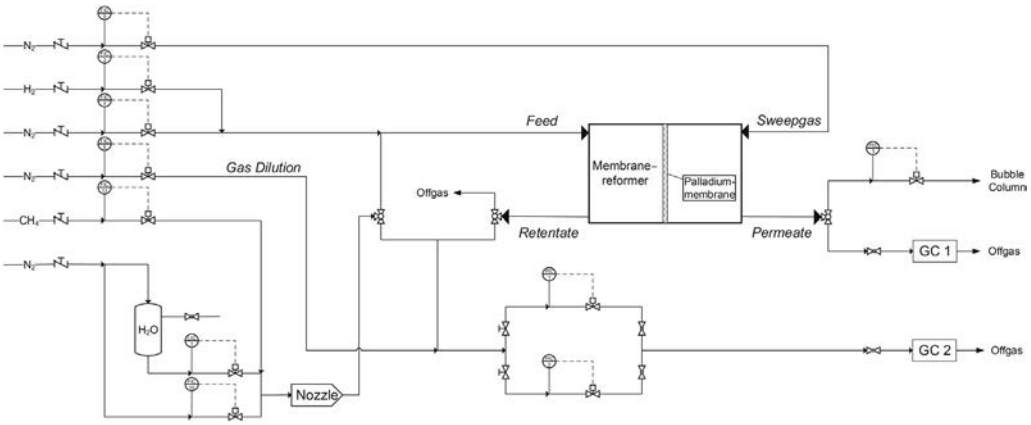


**Fig. 2 – Flow scheme of the test rig used in this work.**

*Reaction conditions and definitions*

The $\mu$ EnH$_2$ancer was tested with a W/F ratio between 0.33 and 1.32 $g_{Cat}h/mol_{CH_4}$, corresponding to a GHSV between 7100 and 29,000 h $^{1}$, and a temperature between 773 and 823 K. Retentate pressures between 6 and 12 bar were applied, and experimental data are reported in the results section. Additionally, 20 bars were applied for several hours without membrane rupture as well, which demonstrated the good mechanical stability of the membrane in combination with the membrane support concept.

The $H_2$ flux $F_{H_2}$ was measured and according to Sieverts' law, the permeance $\prod_{H_2}$ of the membrane was calculated (Eq. (3)).

$$\Pi_{H_2} \quad \frac{Q}{s} \quad \frac{F_{H_2}}{p_{H_2,Ret}^{0.5} \quad p_{H_2,Perm}^{0.5}} \tag{3}$$

In Eq. (3), Q is the permeability, $s$ the thickness of the membrane, and $p_{H_2,Ret}$ and $p_{H_2,Perm}$ are the $H_2$ partial pressures on the retentate and permeate side of the membrane. An indication for the leak tightness of the integrated membrane (membrane and weld seam quality) is the ideal $H_2/N_2$ permselectivity of the membrane S, which is defined as the volume flow of $H_2$ through the membrane divided by the volume flow of $N_2$ at the same temperature and pressure.

$$S \quad \left.\frac{\dot{V}_{H_2}}{\dot{V}_{N_2}}\right|_{T,p} \tag{4}$$

The methane conversion was calculated according to

$$X_{CH_4} \quad \frac{\dot{N}_{CH_4,in} \quad \dot{N}_{CH_4,out}}{\dot{N}_{CH_4,in}} \cdot 100\% \tag{5}$$

in Eq. (5) $\dot{N}$ represents the molar flow rate. The hydrogen recovery is defined as

$$\varphi_{H_2} \quad \frac{\dot{N}_{H_2,Perm}}{\dot{N}_{H_2,Perm} + \dot{N}_{H_2,Ret}} \cdot 100\% \tag{6}$$

For the calculation of the thermodynamic equilibrium conversion of methane as a function of the hydrogen recovery, the Gibbs free energies of the gaseous species, and carbon, were implemented in a Matlab® routine and minimized simultaneously. The effect of hydrogen removal was implemented as a factor in the equilibrium constants.

The CO selectivity was calculated with the following equation.

$$S_{CO} \quad \frac{\dot{N}_{CO}}{\dot{N}_{CH_4,in} \quad \dot{N}_{CH_4,out}} \cdot 100\% \tag{7}$$

An important value is the $H_2$ purity of the permeate. GC analysis was used, and purity of the permeate was calculated based on the detection of carbon containing species in the permeate.

$$\text{Purity} \quad \frac{\dot{N}_{H_2}}{\dot{N}_{H_2} + \dot{N}_{CH_4} + \dot{N}_{CO} + \dot{N}_{CO_2}} \cdot 100\% \tag{8}$$

Note that in Eq. (8), the molar flows only refer to the permeate side and not the retentate/reformate side.

## Results and discussion

*Results of membrane integration*

In the manufacture of a metal based system, laser welding of a few different materials is necessary. One major challenge in laser welding in this circumstance is also the disability to bridge gaps while avoiding filler material. The concavity of the welding seam (Humping effect) can easily lead to bending of the plates in case that the microstructured stack is welded from above. This effect was investigated by variation of the laser parameters and a good solution to avoid this effect was found. The general effect of joining different materials in the reformer system is exemplified in the next paragraph.

Fig. 3(a) shows the detail of a layered stack consisting of austenitic material (pre oxidized 1.4876 (Nicrofer® 3220H) for the top and bottom plates, 1.4401 (stainless steel) for the membrane supports and the Pd foil). The Pd membrane (bright center region) is alloyed into the austenitic material very well. The thermal barrier effect of the pre oxidized Nicrofer® 3220H foils is emphasized by necking of the weld seam at the interfaces between the metal microsieve and the microstructured plates above and below the membrane. In Fig. 3(b) two 50 μm thick ferritic steel foils made of 1.4760 (Crofer 22

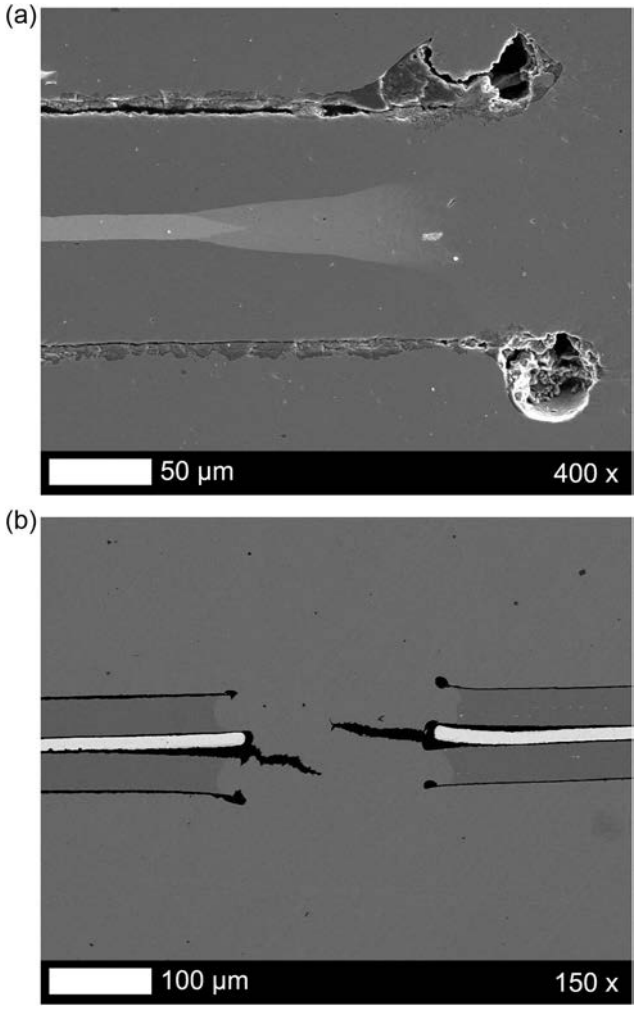


**Fig. 3 – Material scientific issue of laser weld seams. Left: stack consisting of different layers of austenitic material with a Pd membrane. Right: no alloying of the Pd membrane and formation of cracks for a compound of ferritic metal microsieves and microchannel plates in austenitic steel.**

APU) were used instead of austenitic metal microsieves. Obviously the ferritic structure prevents any alloying with the 12.5 µm Pd membrane. Instead, cracks were formed in the welding zone, every time these materials were welded.

### *Characterization of catalyst and membrane*

Due to the limited reaction volume in microstructured reactors, a high volumetric reaction rate is desired. Especially if the catalytic wall coating is thin and the reaction volume is limited, high metal loadings with high surface area can be used that operate at the edge of the pore diffusion limited regime to generate a high volumetric reaction rate. Additionally, a high stability of the catalyst is required, as the catalyst supplied in a wall coating is not as easy replaced as in a fixed bed reactor. In previous works, good activity of reforming catalysts with noble metal loadings between 5 and 30 wt.% was demonstrated [30–32]. However, catalyst coatings based on sol gel often not exceed 10 nm in layer thickness. Therefore, alumina particles were admixed in the sol to increase the catalyst mass per microchannel foil [28]. This is especially important as the ratio of membrane surface area per weight of catalyst is very high in the microchannel membrane reactor.

According to low temperature $N_2$ physisorption measurements, the catalyst showed primarily mesoporosity. The admixed $Al_2O_3$ particles, however, formed a macroporous structure, which was confirmed with Hg porosimetry measurements on support material which has been prepared according to the same recipe as the support layers but in powder form. The total pore area (taking macro and mesopores into account) is 32.2 $m^2/g$ with a pore volume of 0.761 ml/g, resulting in an average pore diameter (4 V/A) of 9.4 nm and a porosity of 74%. $H_2$ chemisorption analysis on $Rh/Al_2O_3$ powder resulted in an average Rh particle diameter of 8 nm and a total accessible active surface area of 9.1 $m^2/g$ (14% dispersion). The chemisorption results are in agreement with particle sizes obtained from TEM analysis and XRD measurements confirmed the presence of $\alpha$ $Al_2O_3$ as dominating phase after calcination.

The activity of the catalyst coating used in this work was evaluated in a microstructured reactor without membrane (not shown here). The fins of the microchannels can serve as a sufficient support for thin Pd based foils up to a retentate pressure of 6 bar [9]. For higher mechanical and thermal stability, however, an additional support is required. Fig. 4 shows a SEM image of the cross section of the microstructured membrane reactor, where the microchannels of the two reaction segments on the feed side, the two supports, the Pd membrane and the microchannels on the permeate side are illustrated.

Before reaction experiments, the nitrogen flux through the membrane modules was determined, which was used as basis for the calculation of the ideal permselectivity (Eq. (4)). In this work, ideal $H_2/N_2$ permselectivities between 1000 and 16,000 at a pressure of 6 bar and a temperature of 773 K were obtained in different membrane modules. The hydrogen permeance and activation energy was first determined at different temperatures and pressures in a microstructured prototype membrane module [9] with identical membrane configuration (12.5 µm Pd membrane with etched microsieve

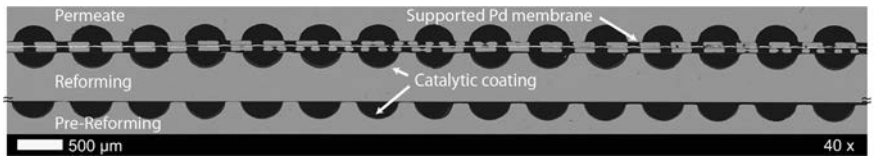


**Fig. 4 – SEM cross section of the microstructured membrane reformer with leak-tight integrated Pd membrane supported by an etched microsieve.**

support integrated via laser welding), and with pure $H_2$ on the feed side and no sweep gas on the permeate side. Leak tight integration of the Pd membranes was achieved in this configuration, appearing that the membrane has full selec tivity towards hydrogen. The results of the hydrogen perme ation experiments in the microstructured prototype membrane module are shown in the Sieverts' plot (Fig. 5), where the hydrogen flux is shown as a function of the dif ference of the square root of the $H_2$ partial pressures on the retentate and the permeate side, according to Eq. (3).

The hydrogen permeation is according to Sieverts' law (*n* value of 0.5), indicated by the dashed line through the origin of the diagram. Compared to $H_2$ flux measurements, where the Pd based membrane is leak tight integrated without an additional support [9], around 30% lower $H_2$ flux was measured with the additional support. This is obviously the influence of the decrease of accessible surface area. However, based on the etched holes of the additional support, the in fluence of the decrease of accessible membrane surface area should be larger. This means in turn, that the support makes additional membrane area accessible for permeation, e.g. the fins of the microstructures. To account for the complex accessible membrane surface, the permeability of the iden tical 12.5 μm Pd membrane derived in Ref. [9] was used and the corresponding membrane surface was calculated. An apparent activation energy of 12.14 kJ/mol was calculated (Fig. 6) that is according to values reported in literature for Pd foils [33].

The following expression for the $H_2$ permeability of the 12.5 μm Pd membrane was derived:

Q 1.58E 07*exp( 1460.2/T) mol/(msPa$^{0.5}$)

### *Results of MSR in the μ-En$H_2$ancer*

*Effect of residence time and steam to carbon ratio*

The methane conversion and selectivity towards CO as a function of residence time (W/F ratio) is shown in Fig. 7 and

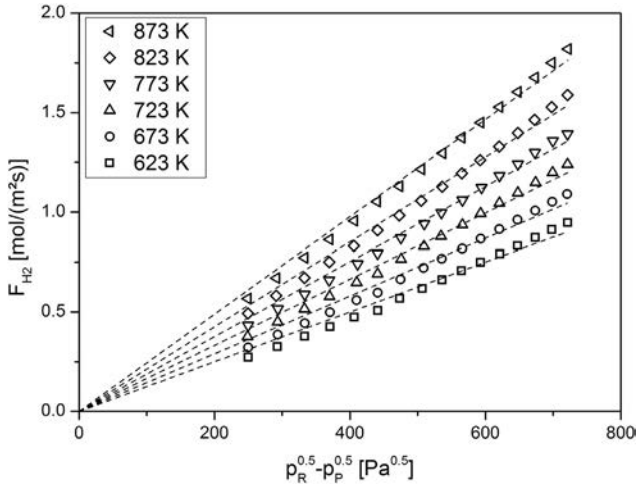


**Fig. 5 – $H_2$ flux as a function of the difference of the square root of the $H_2$ partial pressures at different temperatures.**

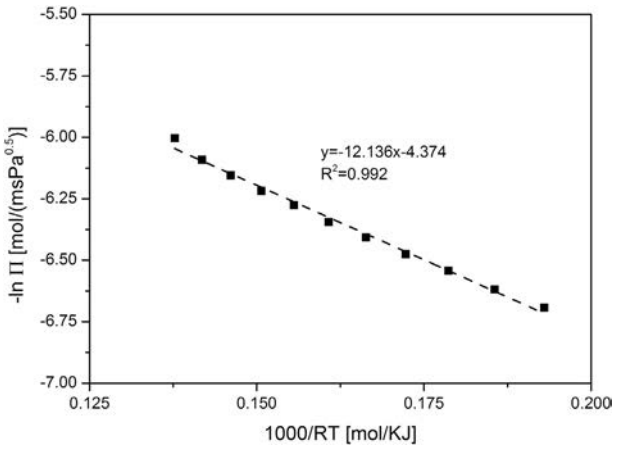


**Fig. 6 – Arrhenius relation between the $H_2$ permeance and the invert of the operation temperature.**

the $H_2$ recovery as a function of W/F ratio is shown in Fig. 8, both at 6 bar feed pressure and a temperature of 773 K in the microstructured membrane reactor.

According to thermodynamics, methane conversion in steam reforming without membrane separation decreases with increasing system pressure. With the Pd membrane, however, the equilibrium is shifted by continuous hydrogen removal and therefore higher methane conversion can be obtained. The methane conversion increases with residence time and a S/C ratio of 4 gave higher methane conversion compared to a S/C ratio of 3. At the lowest weight to feed ratio of 0.33 $g_{Cat}h/mol_{CH_4}$, a S/C ratio of 3, and without sweep gas a methane conversion of 46% was obtained, which is still double the value than for the corresponding equilibrium conversion

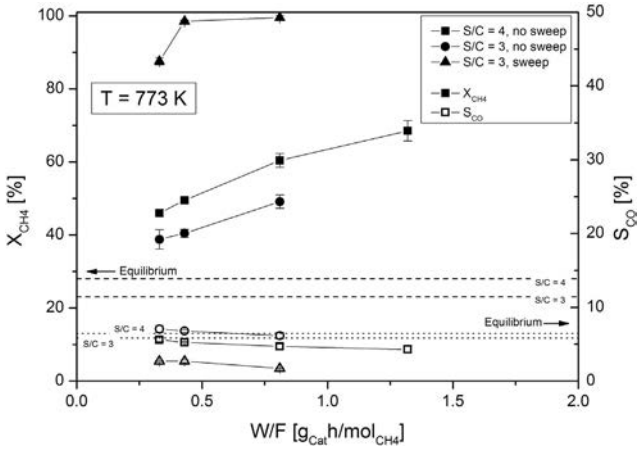


**Fig. 7 – Methane conversion as a function of residence time at a temperature of 773 K, different S/C ratio and a reaction pressure of 6 bar. The dotted and dashed lines indicate the thermodynamic values for CO selectivity and methane conversion, respectively, without membrane separation. Experimental conditions: S/C 4, no sweep gas (squares), S/C 3, no sweep gas (circles), S/C 3, sweep gas (triangles), CO selectivity (open symbols) and $CH_4$ conversion (full symbols).**

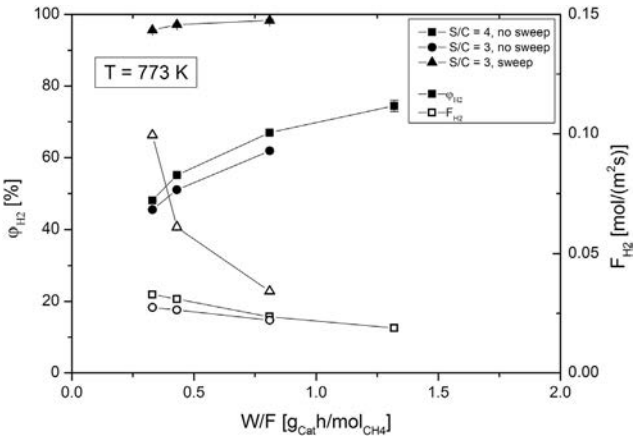


**Fig. 8 – $H_2$ recovery and $H_2$ flux as a function of residence time at a temperature of 773 K, different S/C ratio, and a reaction pressure of 6 bar. Experimental conditions: S/C 4, no sweep gas (squares), S/C 3, no sweep gas (circles), S/C 3, sweep gas (triangles), $H_2$ flux (open symbols) and $H_2$ recovery (full symbols).**

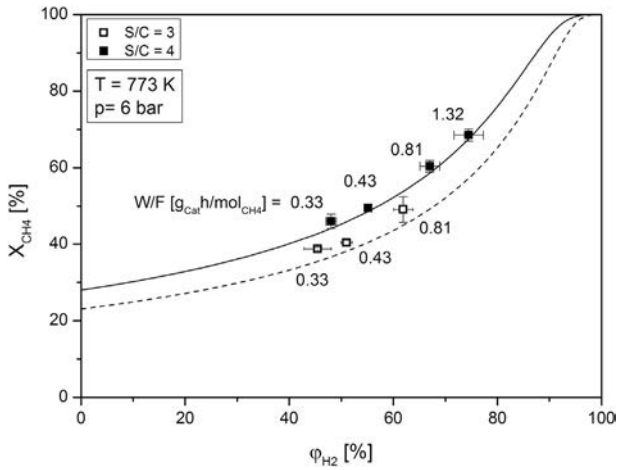


**Fig. 9 – Methane conversion as a function of $H_2$ recovery for different S/C and W/F ratios. Lines are the corresponding equilibrium conditions calculated as a function of hydrogen recovery; dashed line and open symbols for S/C 3, continuous line and full symbols for S/C 4.**

without the membrane. From this doubling of the conversion, it can be assumed, that the partial pressure of hydrogen ex ceeds 1 bar at the end of the "pre reforming" zone and no $H_2$ diffusion from the permeate to the retentate side is decreasing the reactor performance.

The same trends as for conversions were observed for the hydrogen recovery. The higher the residence time the higher the $H_2$ partial pressure in the gas mixture when contacting the membrane, and therefore the higher the hydrogen recovery. In contrast, $F_{H_2}$ increases with decreasing W/F ratio.

The CO selectivity is at the calculated thermodynamic equilibrium but decreases with increasing W/F ratio and increasing hydrogen recovery. This is in accordance with a shift of the WGS reaction towards $CO_2$ by the removal of hydrogen from the reaction zone. The use of sweep gas has a tremendous effect on both conversion and hydrogen recovery. This in dicates that the mass transfer resistance of the etched micro sieve support seems negligible on both sides of the membrane as very low $H_2$ partial pressures on the permeate membrane surface are necessary to obtain such higher hydrogen flux. With the use of sweep gas, full conversion of methane and full hydrogen recovery was obtained at the higher residence times, a temperature of 773 K, and 6 bar retentate pressure. However, sweep gas, or alternatively vacuum is technologically not relevant for the production of high purity hydrogen in decen tralized application, as the separated hydrogen is either diluted or subsequent compression is necessary.

In Fig. 9 the methane conversion measured at different W/F and S/C ratios is shown as a function of $H_2$ recovery. The trend of methane conversion can be well described by the thermo dynamic equilibrium that is calculated with consideration of hydrogen separation, which means that the activity of the catalyst is high enough to catch up with the shift of the thermodynamic equilibrium, see also [34]. The experimental values at a S/C ratio of 3 lie slightly above the thermodynamic equilibrium. This can be explained by a slightly higher determined S/C ratio of around 3.2 from the experiment, while the thermodynamic methane conversion was calculated with the setpoint of the S/C ratio of 3.

*Effect of reaction temperature and pressure*

The influence of reaction pressure on the methane conversion at a constant W/F is shown in Fig. 10. Although the equilibrium conversion decreases with increasing pressure, the actual conversion in the $\mu$ En$H_2$ancer shows the opposite trend due to the effect of $H_2$ removal. Note that for all conditions tested the conversion in the $\mu$ En$H_2$ancer exceeded the equilibrium conversion for a non membrane system.

According to Eq. (3), higher reaction pressures result in an increased hydrogen flux and subsequently in an increased hydrogen recovery (Fig. 11). Therefore, the thermodynamic equilibrium is further shifted with increasing reaction pres sure and higher methane conversions are achieved.

Fig. 12 shows the methane conversion as a function of the $H_2$ recovery $\varphi$ for different pressures and also different tem peratures. The lines stand for the results expected at equilib rium for the case that the fraction $\varphi$ of the produced hydrogen has been removed via the membrane. The points indicate the experimental results actually obtained at 6, 8, 10 and 12 bar retentate pressure. Note that higher pressure improves the permeation flux due to an increase of the $H_2$ partial pressure (provided the activity of the catalyst is high enough), and a higher fraction of hydrogen removed leads to an increased shift of the equilibrium. Therefore, with increasing pressure, at given temperature, the conversion is increased. Higher tem perature likewise improves the conversion as both the equi librium and the kinetics (reaction and permeation) benefit.

The hydrogen purity is not given explicitly for each experiment, but was monitored and checked occasionally during the experiments (if no sweep gas was used). At all times, $H_2$ purity varied between 99.5 and 99.99%.

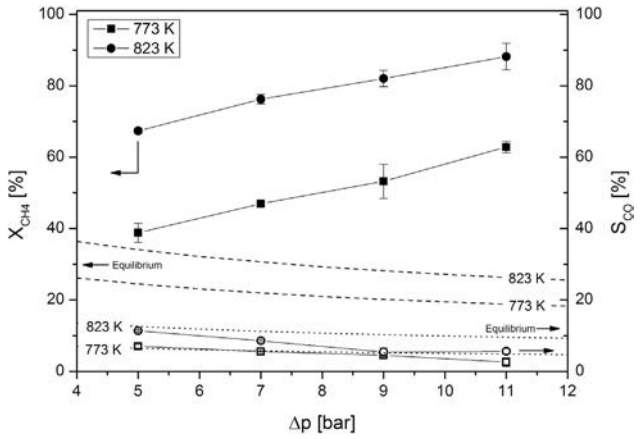


**Fig. 10 – Methane conversion as a function of pressure difference between retentate and permeate side at a *W/F* ratio of 0.33 $g_{Cat}h/mol_{CH_4}$ and a *S/C* ratio of 3. Full symbols: methane conversion, empty symbols: CO selectivity; no sweep gas applied. The dotted and dashed lines indicate the thermodynamic values for CO selectivity and methane conversion, respectively, without membrane separation.**

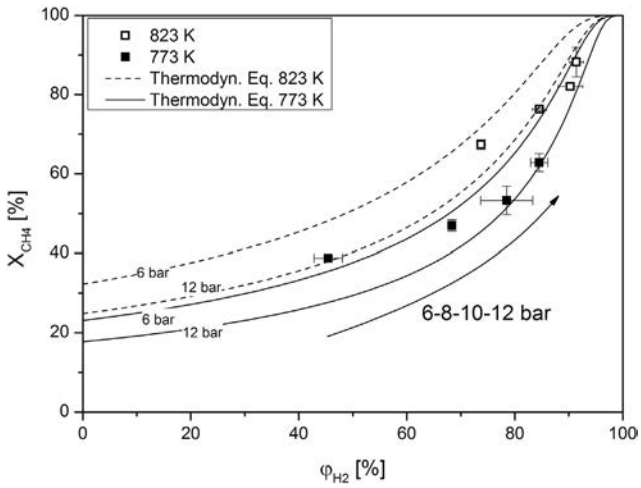


**Fig. 12 – Methane conversion as a function of hydrogen recovery: calculated thermodynamic equilibrium for 6 bar and 12 bar, and 773 K (solid line) and 823 K (dotted line). Experimental values at the reformate pressures of 6-8-10-12 bar (from left to right) at 773 K (full symbols) and 823 K (empty symbols), a constant *W/F* ratio of 0.33 $g_{Cat}h/mol_{CH_4}$ and a *S/C* ratio of 3.**

*Comparison of membrane reactor performance*

The comparison of the performance of the $\mu$ En$H_2$ancer with literature data is difficult, due to often not reported data regarding the catalyst properties such as packing density, the reactor volume and/or membrane area.

The performance of methane steam reforming the micro structured membrane reactor was compared with four different membrane reactor configurations: Laboratory scale single tube membrane reactors reported by Tong et al. [3,6,34] and Uemiya et al. [4], a modular and very compact planar system reported by Hwang et al. [14], and the techni cally most advanced membrane reformer system from Tokyo Gas [15,35]. Table 1 summarizes important reported parame ters of each membrane reactor type tested for hydrogen pro duction from methane steam reforming.

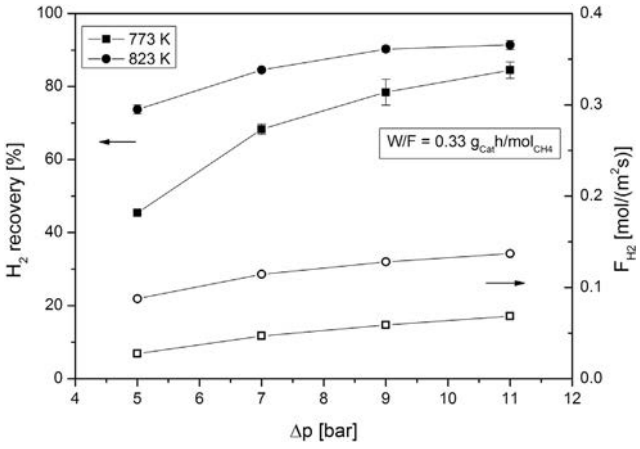


**Fig. 11 – $H_2$ recovery and flux as a function of pressure difference between feed and permeate side at a *W/F* ratio of 0.33 $g_{Cat}h/mol_{CH_4}$ and a *S/C* ratio of 3. Full symbols: $H_2$ recovery, empty symbols: $H_2$ flux; no sweep gas applied.**

In Table 1, the experimental conditions are given, as well as the relations that were considered for comparison, and that are supposed to demonstrate the compactness of the systems, i.e. membrane area per reactor volume, the rate of hydrogen production per reactor volume and the rate of hydrogen pro duction per membrane area. The performance of the micro structured membrane reactor corresponds well with the reported performances of tubular systems regarding $\dot{V}_{H_2}/A_{Pd}$. However, a much lower *W/F* ratio was envisaged in our sys tem, as a highly active Rh based catalytic coating was used. Most important, however, is that a much higher hydrogen production rate per reactor volume was achieved compared with most systems. The reason for the good performance of the microstructured membrane reactor is first of all the very intense contact between catalyst and membrane (<300 μm) and the resulting minimization of concentration gradients from the catalyst towards the membrane surface [9]. Addi tionally a relatively high membrane surface area is incorpo rated in a very compact reactor. Nevertheless, a high membrane area per reactor volume could be achieved in sin gle tube systems as well depending on the calculation. Tong et al. [3,6,34] used a very thin reactor tube with 1.7 cm in diameter. As the tube length was not given, the reactor vol ume was calculated based only on the given catalyst bed height of 8 cm, leading to a high membrane area per reactor volume ratio of up to 110 $m^2/m^3$ and consequently to higher values of $\dot{V}_{H_2}/V_R$ compared to our system. The single tube membrane reformer system of Tong et al. [6] was tested with sweep gas in order to increase the hydrogen flux through the membrane. This led to low $H_2$ recovery, i.e. below 60%. If our microstructured membrane reformer would be operated with sweep gas, a significant increase in hydrogen production rate for the planar system would be expected as well. For practical reason such demonstration was, however, not possible. The

**Table 1 – Overview of different types of membrane reformers available in the literature, membrane thickness $s_{Pd}$, membrane area $A_{Pd}$, type of catalyst, temperature $T$, pressure difference between feed and permeate side $\Delta p$, methane conversion $X_{CH_4}$, hydrogen recovery $\varphi_{H_2}$, weight-to-feed ratio $W/F$, as well as the calculated ratios membrane area per reactor volume, volume flow of hydrogen per reactor volume and volume flow of hydrogen per membrane area.**

| Reference | $s_{Pd}$ [μm] | $A_{Pd}$ [$cm^2$] | Catalyst | $T$ [K] | $\Delta p$ [bar] | $X_{CH_4}$ [%] | $\varphi_{H_2}$ [%] | W/F [g h/$mol_{CH_4}$] | $A_{Pd}/V_R$ [$m^2/m^3$] | $\dot{V}_{H_2}/V_R$ [$Nm^2/(m^3h)$] | $\dot{V}_{H_2}/A_{Pd}$ [$Nm^2/(m^2h)$] |
|---|---|---|---|---|---|---|---|---|---|---|---|
| Uemiya et al. [4] | 20 | 25.1 | Ni based | 773 | 8[a] | 90 | 91 | 64.75 | 39.3 | 230 | 5.9 |
| Tong et al. [6] | 8 | 20 | $Ni/Al_2O_3$ | 823 | 10[b] | 72 | 51 | 74.71 | 110.1 | 1289 | 11.7 |
| Hwang et al. [14] | 6.2 | 33.2 | Ni based | 813 | 20 | 79 | 96 | n.a. | 6.3 | 58 | 9.2 |
| Tokyo Gas [15,35] | 20 | 98918.4 | Ni based | 823 | 8.7[c] | 79 | n.a. | n.a. | 8.1 | 33 | 4.1 |
| $\mu$ $EnH_2$ancer [this work] | 12.5 | 26.3[d] | $Rh/Al_2O_3$ | 823 | 11 | 87 | 92 | 0.33 | 41/66[e] | 472/739[e] | 12.1 |

[a] Sweep gas 500 ml/min Ar ($p_{H_2,Perm} = 0.38$ bar).
[b] Sweep gas 470 ml/min $N_2$.
[c] Vacuum ($p_{H_2,Perm} = 0.4$ bar).
[d] Effective membrane area (across the microchannels).
[e] Optimized membrane module with thinner microstructured foils.

required lower W/F ratio cannot be established in the test rig, and it was not intended to produce diluted hydrogen.

Furthermore, a crucial point in the comparison is that the catalyst and the membrane is influenced by the gas composition on both sides of the membrane. The hydrogen partial pressure on the feed/retentate side of the membrane has to exceed the hydrogen partial pressure on the permeate side, otherwise, back diffusion of hydrogen from the permeate side to the reaction side decreases reaction kinetics and the overall reactor performance. In tubular systems, the catalyst bed usually exceeds the membrane tube. In our planar system, an additional layer, a "pre reforming" section was integrated for the generation of a sufficiently high hydrogen partial pressure. The amount of catalyst in this pre reforming zone has to be well adapted to the requirements of application. Given the case that an elevated pressure on the permeate side is desired, the corresponding hydrogen partial pressure has to be generated at the end of the pre reforming zone.

It must be noted that the heat integration by internal firing is already considered in the calculations for the system of Tokyo Gas with the data available in the literature [15,35], while all the other systems, including the system reported here, are based on laboratory scale experiments with bulky external (electrical) heating. Heat integrated planar microstructured systems can be supposed to keep by minimum half of the hydrogen production rate per reactor volume as catalytic combustion; heat supply usually does not require a 1:1 stack of heating and combustion plates, i.e. the volume for combustion is less than for reforming [32]. In contrast, heat integrated systems based on tubes get much less compact, as multi tubular systems require a certain volume in between the tubes for the circulation of hot flue gas. This, however, has to be experimentally validated in the future.

## Summary and conclusions

A planar and modular microstructured membrane reactor concept ($\mu$ $EnH_2$ancer) is presented. The Pd membranes with an additional etched microsieve support were leak tight integrated with laser welding. Reproducible membrane and membrane support integration for an all austenitic metallic stack was achieved.

The $\mu$ $EnH_2$ancer was tested in methane steam reforming operation at temperatures up to 823 K and retentate pressures up to 12 bar on a highly active $Rh/Al_2O_3$ catalyst. At a W/F ratio of 0.33 $g_{Cal}h/mol_{CH_4}$, a temperature of 823 K, a reformate pressure of 12 bar and without sweep gas, a hydrogen flow above 29 l/h was obtained for a single microstructured membrane reactor module. Due to the very compact system and the apparently subordinated concentration gradients, very high volumetric hydrogen production rates of up to 472 $Nm^3H_2/(m^3h)$ were obtained. Further improvements, such as thinner microstructured foils to obtain an even more compact system are currently under construction.

The modular system shows further advantages such as high membrane area per reactor volume ratios and easy enlargement of capacity by stacking several membrane modules together, depending on the desired hydrogen capacity. Together with the superior heat transfer properties and the possibility of intensive heat integration, very compact technical systems are anticipated.

Throughout the experiments, hydrogen purities higher than 99.5% were obtained and the ideal $H_2/N_2$ permselectivities varied between 16,000 and 1,000 at a temperature of 773 K and 6 bar feed pressure. Higher hydrogen purities (above 99.99%) are anticipated in the future, by using improved Pd membranes and by further improving the welding process.

Further steps are currently conducted to improve the catalyst performance, e.g. preparation of catalyst by flame spray pyrolysis and subsequent inkjet printing with high precision into microchannels [36].

## Acknowledgments

Financial support by the Helmholtz Research School for Energy Related Catalysis is gratefully acknowledged. Further we thank the Institute for Applied Materials and Physics (IAM AWP), KIT, Germany, for the ICP OES measurements. Last but not least we thank Torsten Wunsch (IMVT at KIT) for his inventive ideas regarding the design and construction of the

mounting device and his sophisticated works on laser welding of the microstructured membrane reactor and Robin Dürrschnabel (IMVT) for the fruitful discussion regarding the design of the $\mu$ En$H_2$ancer.

## REFERENCES

[1] Gallucci F, Fernandez E, Corengia P, van Sint Annaland M. Recent advances on membranes and membrane reactors for hydrogen production. Chem Eng Sci 2013;92:40 66.
[2] Dittmar B, Behrens A, Schödel N, Rüttinger M, Franco T, Straczewski G, et al. Methane steam reforming operation and thermal stability of new porous metal supported palladium composite membranes. Int J Hydrogen Energy 2013;38:8759 71.
[3] Tong J, Matsumura Y, Suda H, Haraya K. Experimental study of steam reforming of methane in a thin (6 μM) Pd based membrane reactor. Ind Eng Chem Res 2005;44:1454 65.
[4] Uemiya S, Sato N, Ando H, Matsuda T, Kikuchi E. Steam reforming of methane in a hydrogen permeable membrane reactor. Appl Catal 1991;67:223 30.
[5] Shu J, Grandjean B, Kaliaguine S. Methane steam reforming in asymetric Pd and Pd Ag/porous SS membrane reactors. Appl Catal A Gen 1994;119:305 25.
[6] Tong J, Matsumura Y. Pure hydrogen production by methane steam reforming with hydrogen permeable membrane reactor. Catal Today 2006;111:147 52.
[7] Dittmeyer R, Höllein V, Daub K. Membrane reactors for hydrogenation and dehydrogenation processes based on supported palladium. J Mol Cat A 2001;173:135 84.
[8] Caravella A, Barbieri G, Drioli E. Concentration polarization analysis in self supported Pd based membranes. Sep Purif Technol 2009;66:613 24.
[9] Boeltken T, Belimov M, Pfeifer P, Peters TA, Bredesen R, Dittmeyer R. Fabrication and testing of a planar microstructured concept module with integrated palladium membranes. Chem Eng Process Process Intensif 2013;67:136 47.
[10] Gallucci F, Van Sint Annaland M, Kuipers J. Autothermal of methane with integrated with integrated $CO_2$ capture in a novel fluidized bed membrane reactor. Part 1: experimental demonstration. Top Catal 2008;51:133 45.
[11] Dang N, Gallucci F, van Sint Annaland M. Micro structured fluidized bed membrane reactors: solids circulation and densified zones distribution. Chem Eng J 2014;239:42 52.
[12] Ryi SK, Park JS, Hwang KR, Lee CB, Lee SW. Module configuration in $CO_2$ capture using Pd based composite membranes. Int J Hydrogen Energy 2011;36:13755 69.
[13] Hwang KR, Ryi SK, Lee CB, Lee SW, Park JS. Simplified, plate type Pd membrane module for hydrogen purification. Int J Hydrogen Energy 2011;36:10136 40.
[14] Hwang KR, Lee CB, Ryi SK, Lee SW, Park JS. A multi membrane reformer for the direct production of hydrogen via steam reforming of methane. Int J Hydrogen Energy 2012;37:6601 7.
[15] Kurokawa H, Shirasaki Y, Yasuda I. Energy efficient distributed carbon capture in hydrogen production from natural gas. Energy Procedia 2011;4:674 80.
[16] Lukyanov B, Andreev D, Parmon V. Catalytic reactors with hydrogen membrane separation. Chem Eng J 2009;154:258 66.
[17] Hessel V, Noel T. Ullmann's encyclopedia of industrial chemistry. Wiley VCH; 2012.
[18] Kolb G. Microstructured reactors for distributed and renewable production of fuels and electrical energy. Chem Eng Process Process Intensif 2013;65:1 44.
[19] Mejdell AL, Jøndahl M, Peters TA, Bredesen R, Venvik HJ. Experimental investigation of a microchannel membrane configuration with a 1.4 μm Pd/Ag 23 wt.% membrane effects of flow and pressure. J Membr Sci 2009;327:6 10.
[20] Marra L, Wolbers P, Gallucci F, van Sint Annaland M. Development of a Rh/$ZrO_2$ catalyst for low temperature autothermal reforming of methane in membrane reactors. Catal Today 2013. http://dx.doi.org/10.1016/j.cattod.2013.10.069.
[21] Kundu A, Jang JH, Lee HR, Kim SH, Gil JH, Jung CR, et al. MEMS based micro fuel processor for application in a cell phone. J Power Sources 2006;162:572 8.
[22] Wilhite B, Weiss S, Ying J, Schmidt M, Jensen KF. High purity hydrogen generation in a microfabricated 23 wt.% Ag Pd membrane device integrated with 8:1 LaNi0.95Co0.05/$Al_2O_3$ catalyst. Adv Mater 2006;18:1701 4.
[23] Holladay J, Wang Y, Jones E. Review of developments in portable hydrogen production using microreactor technology. Chem Rev 2004;104:4767 90.
[24] Mitsos A, Barton P, editors. Microfabricated power generation. Wiley VCH Verlag GmbH & Co. KGaA; 2009.
[25] Kazakov NF. Diffusion bonding of materials. Pergamon Press; 1985.
[26] Gietzelt T, Eichhorn L, Wunsch T, Dittmeyer R. Laserschweißen in der Mikroverfahrenstechnik: Möglichkeiten und Grenzen aus werkstofftechnischer Sicht. Galvanotechnik 2013;11:2304 13.
[27] Haas Santo K, Fichtner M, Schubert K. Preparation of microstructure compatible porous supports by sol gel synthesis for catalyst coatings. Appl Catal A Gen 2001;220:79 92.
[28] Ates A, Pfeifer P, Görke O. Thin film catalytic coating of a microreactor for preferential CO oxidaton over Pt catalysts. Chemie Ingenieur Technik 2013;85:664 72.
[29] Piermartini P, Schuhmann T, Pfeifer P, Schaub G. Water gas shift in microreactors at elevated pressure: platinum based catalyst systems and pressure effects. Top Catal 2011;54:967 76.
[30] Wang Y, Chin YH, Rozmiarek RT, Johnson BR, Gao Y, Watson J, et al. Highly active and stable Rh/MgO $Al_2O_3$ catalysts for methane steam reforming. Catal Today 2004;98:575 81.
[31] Görke O, Pfeifer P, Schubert K. Kinetic study of ethanol reforming in a microreactor. Appl Catal A Gen 2009;360:232 41.
[32] Thormann J, Pfeifer P, Schubert K, Kunz U. Reforming of diesel fuel in a micro reactor for APU systems. Chem Eng J 2009;135:S74 81.
[33] Morreale BD, Ciocco MV, Enick RM, Morsi BI, Howard BH, Cugini AV, et al. The permeability of hydrogen in bulk palladium at elevated temperatures and pressures. J Membr Sci 2003;212:87 97.
[34] Tong J, Matsumura Y. Effect of catalytic activity on methane steam reforming in hydrogen permeable membrane reactor. Appl Catal A Gen 2005;286:226 31.
[35] Shirasaki Y, Tsuneki T, Ota Y, Yasuda I, Tachibana S, Nakajima H, et al. Development of membrane reformer system for highly efficient hydrogen production from natural gas. Int J Hydrogen Energy 2009;34:4482 7.
[36] Lee S, Boeltken T, Mogalicherla AK, Gerhards U, Pfeifer P, Dittmeyer R. Inkjet printing of porous nanoparticle based catalyst layers in microchannel reactors. Appl Catal A Gen 2013;467:69 75.